Journal of Solid State Chemistry 183 (2010) 451–457

Contents lists available at ScienceDirect

Journal of Solid State Chemistry

journal homepage: www.elsevier.com/locate/jssc

Homogeneous one-dimensional structured $Tb(OH)_3:Eu^{3+}$ nanorods: Hydrothermal synthesis, energy transfer, and tunable luminescence properties

Jun Yang [a,b], Guogang Li [b], Chong Peng [b], Chunxia Li [b], Cuimiao Zhang [b], Yong Fan [b], Zhenhe Xu [b], Ziyong Cheng [b], Jun Lin [b,*]

[a] School of Chemistry and Chemical Engineering, Southwest University, Chongqing 400715, PR China
[b] State Key Laboratory of Application of Rare Earth Resources, Changchun Institute of Applied Chemistry, Chinese Academy of Sciences, Changchun 130022, PR China

ARTICLE INFO

Article history:
Received 26 August 2009
Received in revised form
29 November 2009
Accepted 5 December 2009
Available online 16 December 2009

Keywords:
Hydrothermal synthesis
Nanorods
Energy transfer
Luminescence

ABSTRACT

Nearly monodisperse, homogeneous and well-defined one-dimensional $Tb_{(1-x)}(OH)_3:xEu^{3+}$ (x=0–3 mol%) nanorods have been prepared through hydrothermal method. The size of the $Tb(OH)_3:Eu^{3+}$ rods could be modulated from nano- to micro-scale by using different amount of ammonia solution. They present highly crystallinity in spite of the moderate reaction temperature. Under ultraviolet excitation into the $f \rightarrow f$ transition of Tb^{3+} at 382 nm, $Tb(OH)_3$ samples show the characteristic emission of Tb^{3+} corresponding to $^5D_4 \rightarrow {}^7F_{6,\ 5,\ 4,\ 3}$ transitions; whereas $Tb(OH)_3:Eu^{3+}$ samples mainly exhibit the characteristic emission of Eu^{3+} corresponding to $^5D_0 \rightarrow {}^7F_{1,\ 2,\ 4}$ transitions due to an efficient energy transfer occurs from Tb^{3+} to Eu^{3+}. The increase of Eu^{3+} concentration leads to the increase of the energy transfer efficiency from Tb^{3+} to Eu^{3+}. The PL colors of $Tb(OH)_3:xEu^{3+}$ phosphors can be easily tuned from green, yellow, orange, to red by changing the doping concentration (x) of Eu^{3+}.

1. Introduction

Inorganic phosphor materials based on rare earth (RE) compounds and RE ions doped compounds have been widely used in modern lighting and display fields, such as fluorescent lamps, cathode-ray tubes, field emission displays, and plasma display panels because of their abundant emission colors resulting from the 4*f* electronic shells [1–5]. Recently, the request for light-emitting-diode (LED) converted phosphors has triggered active research efforts in the investigation of single-phased light-emitting phosphors via chemical approaches [6]. It is well-known that the energy transfer plays an important role in luminescent materials both from theoretical and practical points of view [3,5]. It has been recognized that the luminescence intensities of various rare earth ions can be enhanced or quenched by the energy transfer from other codoped rare earth ions [3,7]. For example, the emission intensity of Tb^{3+} is greatly enhanced by an energy transfer from Ce^{3+} in $LaPO_4:Ce^{3+}$, Tb^{3+} phosphor, leading it to be an efficient luminescent material for fluorescent lamps [3]. It has also been demonstrated that as a result of the energy transfer phenomena it is possible to reduce the threshold energy of laser oscillation in some solid laser materials [8]. As the most frequently used activator ions in luminescent materials, the Eu^{3+} and Tb^{3+} mainly show emissions due to transitions of $^5D_0 \rightarrow {}^7F_J$ (J=1, 2, 3, 4) in the red region and $^5D_4 \rightarrow {}^7F_J$ (J=6, 5, 4, 3) in the green region, respectively [3]. Moreover, it is well-known that an effective energy transfer can take place from Tb^{3+} to Eu^{3+} in several hosts, such as tungstates [9], zeolite-Y [10], yttria [11], porous silicon [12], and molybdates [13]. In these works, there is a common feature that the Tb^{3+} and Eu^{3+} ions are codoped in the third-party hosts as activators. So far, only limited information is available on Eu^{3+}-doped terbium-based hosts [14,15].

One-dimensional (1D) nanostructures, including nanorods, nanowires, nanotubes, and nanoprisms, have attracted extensive synthetic interest over the past several years due to their potential applications in a wide range of fields [16–18]. Up to now, many kinds of novel 1D structured materials have been successfully synthesized, such as III–V [19] and II–VI semiconductors [20,21] and elemental and oxide nanowires/nanorods [22,23]. The widely used method to prepare 1D structures is the catalyst- and template-based method in which the catalysts act as the energetically favored sites for the adsorption of gas reactants while the templates are used to direct the growth of the 1D structure. The formation of 1D structures therefore depends greatly on the selection of suitable catalysts or templates, which involves a complicated process and may result in impurities in the

* Corresponding author. Fax: +86 431 85698041.
E-mail address: jlin@ciac.jl.cn (J. Lin).

0022-4596/$ - see front matter © 2009 Elsevier Inc. All rights reserved.
doi:10.1016/j.jssc.2009.12.005

products. One can overcome these difficulties by developing solution-phase methods for direct growth of the 1D nanostructure without involving catalysts or templates [24]. Enlightened by the recent studies on the 1D nanostructure that can be prepared by evaporating the desired metal oxide powders at high temperatures [25], we believe that the 1D nanostructure might be prepared via a dissolution-recrystallization process in solution.

As we know, with the advantages of high purity and good homogeneity, the hydrothermal synthesis method is an important technology for the preparation of low-dimension nanostructures of anisotropic nanomaterials [26]. The advantage of the hydrothermal method resulting from the fact that neither catalyst nor template is required makes it another choice besides the template method. In addition, starting materials in hydrothermal method can be mixed at molecular level and the reaction temperature for the formation of desired products is relatively low. Also hydrothermal method can prevent oxidation of some ions during synthesis process, just like trivalent terbium ($Tb^{3+} \rightarrow Tb^{4+}$) [15], which inevitably leads to loss of luminescence. Up to now, there are many reports about 1D structured rare earth hydroxides and oxides obtained by the hydrothermal method and postcalcining process, respectively [17,27–31]. Once rare earth compounds were fabricated in the form of a 1D nanostructure, they would be expected to be highly functionalized materials as a result of both shape-specific and quantum confinement effects, acting as electrically, magnetically, or optically functional host materials as well. Unfortunately, so far little attention has been paid to synthesis and luminescent properties of 1D structured $Tb(OH)_3$ and $Tb(OH)_3$:Eu^{3+} nanorods [32–34], and the corresponding energy transfer from Tb^{3+} to Eu^{3+} in $Tb(OH)_3$ host has not been realized and reported. $Tb(OH)_3$ is of hexagonal crystal structure, which may be favorable for the energy transfer from Tb^{3+} to Eu^{3+} [14,15].

Accordingly in this article, we choose to synthesize of $Tb_{(1-x)}(OH)_3$:xEu^{3+} (x=0–1) nanorod phosphors directly by a simple hydrothermal method without protection under reductive ambience for two main specific reasons. On the one hand, we attempted to control the size, morphology, and crystallinity of $Tb(OH)_3$:Eu^{3+} nanocrystals by the use of simple hydrothermal method and tried to explain it is also a good way to prepare 1D structured material. On the other hand, Tb^{3+} and Eu^{3+} themselves are both excellent green and red light emitting centers in luminescent materials, respectively. The energy transfer of $Tb^{3+} \rightarrow Eu^{3+}$ also can occur in terbium-based host $Tb(OH)_3$, which allows the fine-tuning of the emission chromaticity from green, yellow, orange, to red because of different composition of emissions of Tb^{3+} and Eu^{3+} resulted from different energy efficiency at different doping concentration of Eu^{3+}.

2. Experimental section

Materials: The initial chemicals in this work, Tb_4O_7 and Eu_2O_3 (both with purity of 99.99%, Changchun Applied Chemistry Science and Technology Limited, China), HNO_3, $NH_3 \cdots H_2O$, and ethanol (all with purity of analytical reagent, Beijing Fine Chemical Company, China), were used without further purification.

Preparation: The $Tb_{(1-x)}(OH)_3$:xEu^{3+} (x=0–1) samples were all prepared by a simple hydrothermal process. First, Tb_4O_7 and Eu_2O_3 were dissolved in dilute HNO_3, respectively, resulting in the formation of a colorless stock solution of $Tb(NO_3)_3$ with 0.2 mol/L and a colorless solution of $Eu(NO_3)_3$ with 0.0002 and 0.02 mol/L, respectively. In a typical synthesis, the stoichiometric amounts of $Tb(NO_3)_3$ and $Eu(NO_3)_3$ solution were mixed under stirring, and then deionized water was added to the above mixture to reach 41 mL for total volume of H_2O. The solution was stirred for another 15 min to form a clear aqueous solution. Then certain amount (1, 1.3, 1.9, and 2.8 mL) of $NH_3 \cdot H_2O$ (25 wt%, A. R.) was introduced dropwise to the vigorously stirred solution. After additional agitation for 30 min, the as-obtained white colloidal precipitate was transferred to a 50 mL autoclave, sealed, and heated at 200 °C for 30 h. It was then cooled to room temperature naturally. The products were separated by centrifugation, washed with ethanol, and deionized water for several times, and dried in atmosphere at 80 °C for 6 h.

Characterization: The phase purity and crystallinity of the samples were examined by powder X-ray diffraction (XRD) performed on a Rigaku-Dmax 2500 diffractometer with Cu $K\alpha$ radiation (λ=0.15405 nm). The morphology and structure of the samples were inspected using a field emission scanning electron microscopy (FE-SEM, XL 30, Philips) and a transmission electron microscope. Low-resolution transmission electron microscopy (TEM) images and selective area electron diffraction (SAED) patterns were obtained using a JEOL 2010 transmission electron microscope operating at 150 kV. Highresolution transmission electron microscopy (HRTEM) images were performed using FEI Tecnai G2 S-Twinwere with a field emission gun operating at 200 kV. Images were acquired digitally on a Gatan multiple CCD camera. Photoluminescence (PL) excitation and emission spectra were recorded with a Hitachi F-4500 spectrophotometer equipped with a 150Wxenon lamp as the excitation source at room temperature. The luminescence decay curves and the time-resolved emission spectrum were obtained from a Lecroy Wave Runner 6100 Digital Osilloscope (1 GHz) using a tunable laser (pulse width=4 ns, gate=50 ns) as the excitation (Contimuum Sunlite OPO). All of the measurements were performed at room temperature.

3. Results and discussion

3.1. Phase

Both $Tb(OH)_3$ and $Eu(OH)_3$ exhibit very similar X-ray diffraction patterns with hexagonal structure so that we can expect their full miscibility. Therefore, the whole solid solution $Tb_{(1-x)}(OH)_3$:-xEu^{3+} from x=0 to 1 is expected to form. Here we only take $Tb(OH)_3$:1 mol%Eu^{3+} nanorods (2.8 mL ammonia solution) as a typical example due to limited space. All diffraction peaks for as-formed samples in Fig. 1 can be readily indexed to pure hexagonal of $Tb(OH)_3$ [space group: $P63/m(176)$] according to the Joint Committee on Powder Diffraction Standards (JCPDS) file no. 83-2038. The calculated lattice constants using Jade 5.0 program, a=b=6.329 Å and c=3.611 Å, are well compatible with the literature values (a=b=6.315 Å and c=3.603 Å) from the

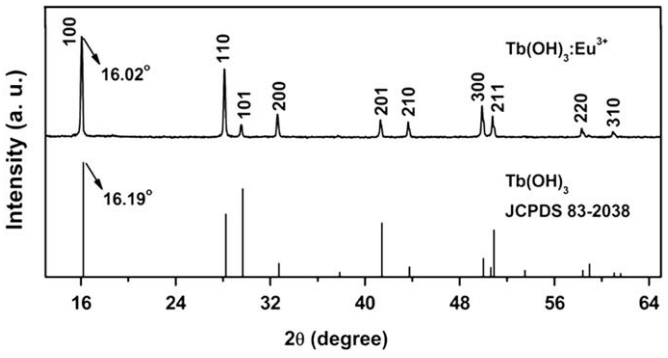

Fig. 1. XRD pattern of $Tb(OH)_3$:1 mol%Eu^{3+} nanorods. The standard data for $Tb(OH)_3$ (JCPDS card 83-2038) is also presented in the figure for comparison.

standard card (JCPDS no. 83-2038). It is worth noting that when the Tb^{3+} was substituted by the Eu^{3+}, the lattice constants become a little bigger and the corresponding XRD peaks move to a lower degree [15] (arrows in Fig. 1). No additional peaks of other phases have been found in Fig. 1, indicating that Eu^{3+} has been effectively built into the $Tb(OH)_3$ host lattice. The relative intensity ratio of the diffraction peak (110) for $Tb(OH)_3$:1 mol% Eu^{3+} products is much higher than the conventional value from JCPDS no. 83-2038, indicating that the samples tend to be preferentially oriented along the *c*-axis due to the natural growing habit of forming 1D morphology during growth process of rare earth hydroxides [26]. What is more, high crystallinity can be obtained at a relatively low temperature [35,36]. This is important for phosphors, because high crystallinity always means less traps and stronger luminescence. In addition, Tb^{3+}-based compound was prepared through hydrothermal process without reductive ambience for protection, which is also one of the merits for preparation of $Tb(OH)_3$:Eu^{3+} phosphors via the present hydrothermal process [15].

3.2. Structure and morphology

The amount of ammonia solution $NH_3 \cdot H_2O$ (25 wt%, A. R.) added to solution for reaction has great effects on the size of the hydrothermal products. Fig. 2a is a wide-field FESEM image observed from the as-formed $Tb(OH)_3$:1 mol% Eu^{3+} with 2.8 mL of $NH_3 \cdot H_2O$, clearly indicating that the $Tb(OH)_3$:Eu^{3+} product consists of nanorods in 100% morphological yield with diameters of ~60 nm and lengths of ~350 nm. When the amount of ammonia solution $NH_3 \cdot H_2O$ decreased from 2.8, 1.9, 1.3 to 1.0 mL with decrease in the pH values of colloidal solution, the size of the $Tb(OH)_3$:Eu^{3+} products increased from nanometer to micrometer scale. Namely, ~80 nm in diameter and ~740 nm in length with 1.9 mL of $NH_3 \cdot H_2O$ (Fig. 2b); ~145 nm in diameter and ~1200 nm in length with 1.3 mL of $NH_3 \cdot H_2O$ (Fig. 2c); ~340 nm in diameter and ~5000 nm in length with 1.0 mL of $NH_3 \cdot H_2O$ (Fig. 2d). For the as-obtained products, from nanorods to microrods (Fig. 2a–d), we observe that the mean aspect ratios are 5.8, 9.25, 8.27, 14.7, respectively, which increases as the pH value decreases. This can be explained by the complex interaction and balance between the chemical potential and the rate of ionic motion. A higher pH value implies a higher OH^- ion concentration and a higher chemical potential in solution. A high chemical potential is preferable for the growth of higher aspect ratio 1D structure; however, higher OH^- ion concentrations may greatly reduce the Tb^{3+} ion concentration in solution, which is restricted by the value of K_{sp} for $Tb(OH)_3$, and thus reduce the rate of ionic motion, giving a low aspect ratio. The phenomenon is similar to the connection of pH values with the aspect ratio of 1D structures in the work of Li and our previous work [17,26]. Furthermore, each nanorod or microrod has a uniform diameter along its entire length and the $\pm c$-axis (corresponding to the growth direction of the rods) ends project out (Inset in Fig. 2d), indicating the growth anisotropy in the $\pm c$-axis is strictly maintained throughout the process. In particular, no branching is observed, which implies that the $Tb(OH)_3$:Eu^{3+} nanorods or microrods were grown from spontaneous nucleation with high crystal perfection [26,37].

Although the exact mechanism for the formation of these rods is still unclear, it is believed that the growth of the rod-like morphology is not assisted by a catalyst or directed by a template. It is well-known that most of the lanthanide hydroxides have hexagonal crystal structures, just like that of ZnO, which is well-known for its anisotropic growth nature. In this case, it is likely that the anisotropic growth of rod-like $Tb(OH)_3$ is governed by a solution-solid (SS) process [26,37,38]. First, the $Tb(OH)_3$ colloid particles are partially dissolved in water to form a metastable supersaturated solution under hydrothermal conditions, then large numbers of the $Tb(OH)_3$ seeds formed through a homogeneous nucleation process, subsequently recrystallizing and growing into uniform, crystalline rod-like structure along the *c*-axis because of a highly anisotropic structure. Similar formation mechanism for other lanthanide hydroxide had been reported in our previous work [26].

Fig. 3a shows a typical TEM image of as-prepared $Tb(OH)_3$:1 mol% Eu^{3+} with 2.8 mL of $NH_3 \cdot H_2O$, clearly showing that the product is entirely composed of relatively uniform nanorods with same size shown in the SEM image (Fig. 2a). Fig. 3b shows the SAED pattern recorded from an area containing a large number of nanorods. The rings in the SAED pattern can be indexed as the (002), (201), (110), and (100) reflections of the

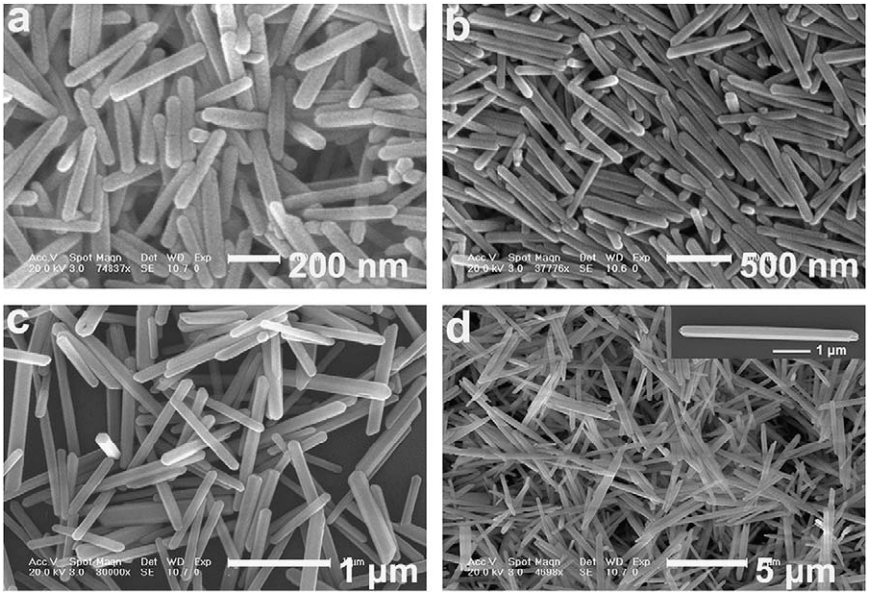

Fig. 2. SEM images of the as-formed $Tb(OH)_3$:1 mol%Eu^{3+} with 2.8 (a), 1.9 (b), 1.3 (c) and 1.0 mL (d) of ammonia solution $NH_3 \cdot H_2O$, respectively.

hexagonal $Tb(OH)_3$, in good agreement with the XRD result. Fig. 3c shows the corresponding HRTEM image of $Tb(OH)_3$:1 mol% Eu^{3+} nanorods recorded along the [110] direction [26,39]. It can be seen that the corresponding (110) plane is oriented parallel to the nanorod growth direction (the *c*-axis) due to the clearly resolved interplanar distance $d_{(110)}$=0.320 nm; the nanorods grow along the [001] direction (the *c*-axis).

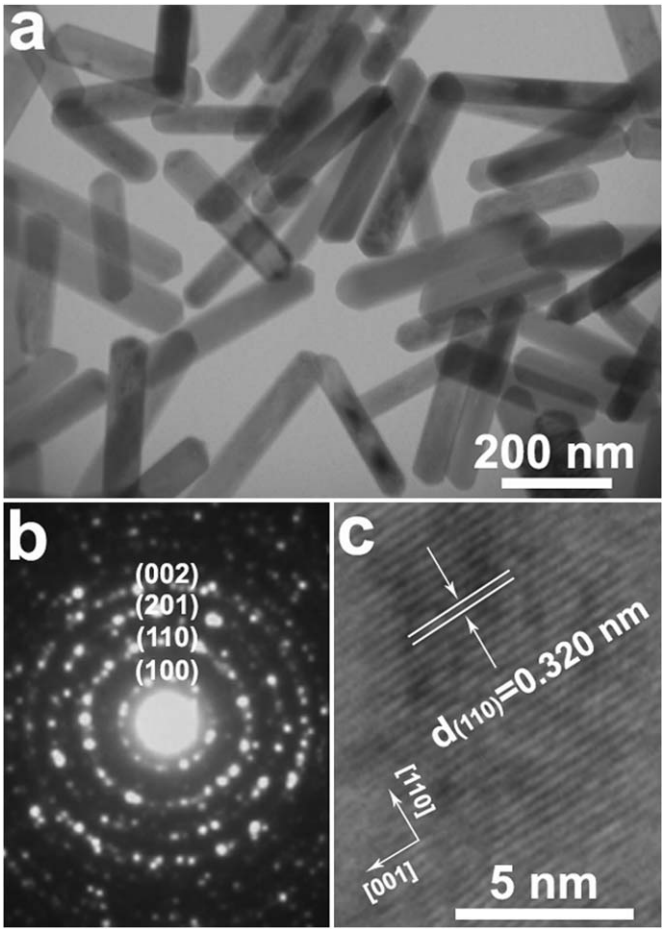

Fig. 3. A typical TEM image of as-prepared $Tb(OH)_3$:1 mol%Eu^{3+} with 2.8 mL of $NH_3 \cdot H_2O$ (a), SAED pattern (b), HRTEM image (c).

3.3. Photoluminescence properties

The $Tb(OH)_3$ sample emits bright-green light under UV excitation. Fig. 4 shows the excitation (a) and emission (b) spectra of the sample. The excitation spectrum of $Tb(OH)_3$ monitored with 543 nm emission of Tb^{3+} ($^5D_4 \rightarrow {}^7F_5$) consists the characteristic $f \rightarrow f$ transition lines within the Tb^{3+} $4f^8$ configuration in the ultraviolet wavelength region, assigned as the transitions from the $^7F_6$ ground state to the different excited states of Tb^{3+}, that is, 307 nm ($^5H_6$), 322 nm ($^5D_0$), 345 nm ($^5G_2$), 356 nm ($^5D_2$), 371 nm ($^5G_6$), 382 nm ($^5D_3$), and 488/492 nm ($^5D_4$), respectively [40]. Upon excitation into the $^7F_6 \rightarrow {}^5D_3$ transition at 382 nm, the obtained emission spectrum (Fig. 4b) of $Tb(OH)_3$ consists of $f \rightarrow f$ transition lines within $4f^8$ electron configuration of Tb^{3+}, that is, $^5D_4 \rightarrow {}^7F_6$ (491 nm) in the blue region and $^5D_4 \rightarrow {}^7F_5$ (543 nm) in the green region, as well as $^5D_4 \rightarrow {}^7F_4$ (583 nm) and $^5D_4 \rightarrow {}^7F_3$ (621 nm) in the red region. The strongest one is located at 543 nm corresponding to $^5D_4 \rightarrow {}^7F_5$ transition of Tb^{3+}. The decay curve (Fig. 5a) for the luminescence of Tb^{3+} (monitored by $^5D_4 \rightarrow {}^7F_5$, 543 nm) can be well fitted into single exponential function as $I = I_0 exp(-t/\tau)$, and the lifetime τ for the $^5D_4$ state of Tb^{3+} is determined to be 0.37 ms in $Tb(OH)_3$ sample. In pure terbium hydroxide, a severe concentration quenching should also occur decreasing considerably the luminescence, so the value of lifetime for Tb^{3+} is relatively low.

However, the green emission of the $Tb(OH)_3$ host material changes greatly when doping Eu^{3+} in it. The $Tb(OH)_3$:1 mol%Eu^{3+} sample shows a red emission under UV excitation. Fig. 4 shows the excitation (c) and emission (d) spectra of the sample. The excitation spectrum recorded at the 591 nm ($^5D_0 \rightarrow {}^7F_1$) of Eu^{3+} is composed exclusively of the excitation bands of Tb^{3+}, which is identical with the excitation spectrum of Tb^{3+} in $Tb(OH)_3$ (Fig. 4a), except for some minor $f \rightarrow f$ transition lines within the Eu^{3+} $4f^6$ configuration (398 nm, $^7F_0 \rightarrow {}^5L_6$; 419 nm, $^7F_0 \rightarrow {}^5D_3$; and 469 nm, $^7F_0 \rightarrow {}^5D_2$, as assigned in Fig. 4(c). The presence of the excitation bands and lines of Tb^{3+} in the excitation spectrum monitored with Eu^{3+} emission clearly indicates that an energy transfer has occurred from Tb^{3+} to Eu^{3+} in the $Tb(OH)_3$: 1 mol% Eu^{3+} sample. Excitation into the $^7F_6 \rightarrow {}^5D_3$ transition of Tb^{3+} excitation band at 382 nm yields mainly the emission of Eu^{3+} ($^5D_0 \rightarrow {}^7F_1$ at 591 nm, $^5D_0 \rightarrow {}^7F_2$ at 616 nm, and $^5D_0 \rightarrow {}^7F_4$ at 695 nm), together with the very weak emission of Tb^{3+} ($^5D_4 \rightarrow {}^7F_5$ at 543 nm and $^5D_4 \rightarrow {}^7F_6$ at 491 nm, green arrows), as shown in part d of Fig. 4. This is further indicative of the energy transfer from Tb^{3+} to Eu^{3+} in $Tb(OH)_3$:1 mol% Eu^{3+} sample.

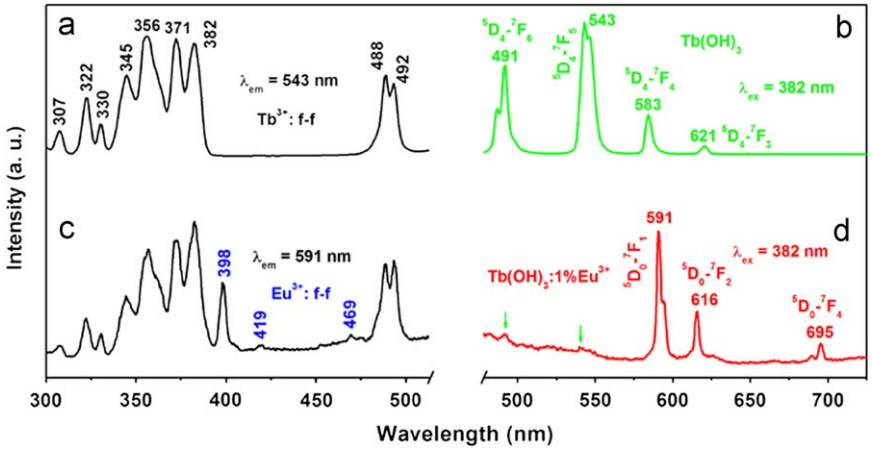

Fig. 4. Excitation (a, c) and emission (b, d) spectra of the $Tb(OH)_3$ (a, b) and $Tb(OH)_3$:1 mol%Eu^{3+} (c, d), respectively.

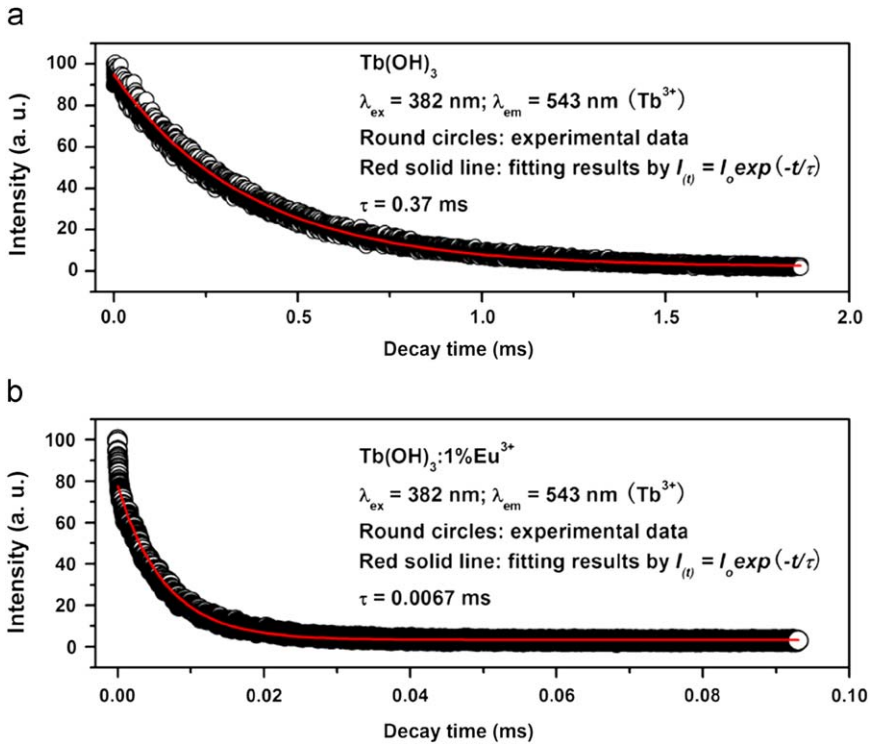

Fig. 5. The decay curves for the luminescence of Tb^{3+} in $Tb(OH)_3$ (a) and $Tb(OH)_3$:1 mol%Eu^{3+} (b).

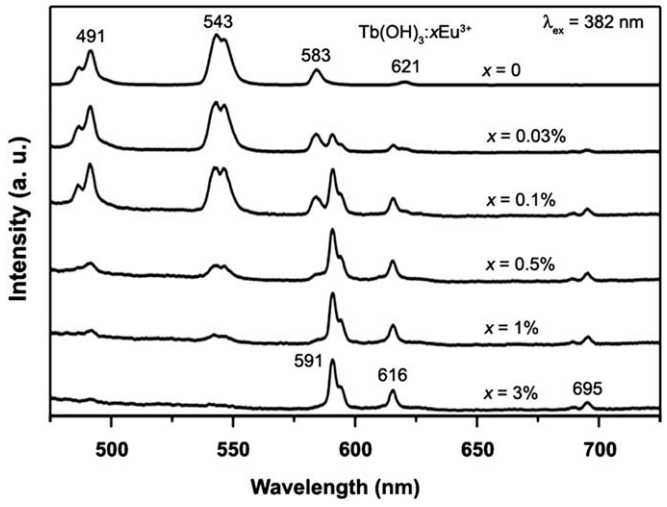

Fig. 6. Emission spectra of $Tb(OH)_3$:xEu^{3+} (x=0–3 mol%) under 382 nm excitation.

Similar to the single exponential luminescence decay of Tb^{3+} in $Tb(OH)_3$ sample, the luminescence decay curve of Tb^{3+} (Fig. 5b) in the $Tb(OH)_3$:1 mol% Eu^{3+} sample can also be well-fitted into single exponential function, and the lifetime τ for the $^5D_4$ state of Tb^{3+} is determined to be 0.0067 ms in the $Tb(OH)_3$:1 mol% Eu^{3+} sample, which is much shorter than that in $Tb(OH)_3$ (0.37 ms). Obviously, the shortening of the lifetime in $Tb(OH)_3$:1 mol% Eu^{3+} with respect to $Tb(OH)_3$ is due to the occurrence of the energy transfer from Tb^{3+} to Eu^{3+} in the former sample [14,15,41,42].

Fig. 6 shows the emission spectra of $Tb(OH)_3$: xEu^{3+} (x=0–3 mol%) under 382 nm excitation. In the undoped $Tb(OH)_3$ (x=0), only the characteristic emissions of Tb^{3+} are observed. With the doping of Eu^{3+} (x=0.03 mol%), besides Tb^{3+} emissions, we can also observe the characteristic emissions of Eu^{3+} (591 nm). With the increase of Eu^{3+} concentration, the luminescence of Tb^{3+} begins to decrease, and the luminescence of Eu^{3+} increases further. This indicates an efficient energy transfer occurs from Tb^{3+} to Eu^{3+}. Also, such energy transfer behavior shows that the as-synthesized $Tb(OH)_3$:xEu^{3+} is not a mixture of $Tb(OH)_3$ and $Eu(OH)_3$ [14]. Otherwise, the $Tb^{3+} \rightarrow Eu^{3+}$ energy transfer can not occur in the separated phases. The energy transfer efficiency from Tb^{3+} to Eu^{3+} depends strongly on the doping concentration of Eu^{3+} in $Tb(OH)_3$ host, just like that of $LaPO_4$:Ce^{3+}, Tb^{3+} [43]. The energy transfer efficiency from a donor (Tb^{3+}) to an acceptor (Eu^{3+}) can be calculated according to the formula $\eta_{ET}=1-\tau/\tau_0$, where τ and τ_0 are the corresponding luminescence lifetimes of the donor (Tb^{3+}) in the presence and absence of the acceptor (Eu^{3+}) for the same donor concentration (Here, we overlooked tiny change of the donor (Tb^{3+}) concentration) [43]. We investigated systematically the energy transfer efficiencies of $Tb^{3+} \rightarrow Eu^{3+}$ in $Tb(OH)_3$: xEu^{3+} (x=0–3 mol%) systems by calculating the lifetimes of Tb^{3+}, and the results are listed in Table 1. Clearly, it is known from Table 1 that with the increase of Eu^{3+} concentration, the energy transfer efficiency from Tb^{3+} to Eu^{3+} increases gradually. This is because the energy transfer probability from Tb^{3+} to Eu^{3+} is proportional to R^{-6} (R is the average distance between Tb^{3+} and Eu^{3+}) [44]. When the Eu^{3+} concentration is equal to 3 mol% mol of Tb^{3+}, η_{ET} reaches the value as high as 99%.

Table 1
Energy transfer efficiency (η_{ET}) from Tb^{3+} to Eu^{3+}, the life time τ for the luminescence of Tb^{3+} in the $TbBO_3$:xEu^{3+} (x=0–1 mol%) samples upon excitation into the Tb^{3+} excitation band with 382 nm.

Eu^{3+} (mol%)	0 (%)	0.03 (%)	0.1 (%)	0.5 (%)	1 (%)	3 (%)
$\tau(Tb^{3+})$, 542 nm (μs)	370	120	50	10	6.7	2.3
$\eta_{ET(Tb \rightarrow Eu)}$ (%)	–	67	86	97	98	99

The PL colors can be tuned from green, yellow, orange, to red by changing the doping concentration of Eu^{3+} ions due to different energy transfer efficiencies at different Eu^{3+} concentra-

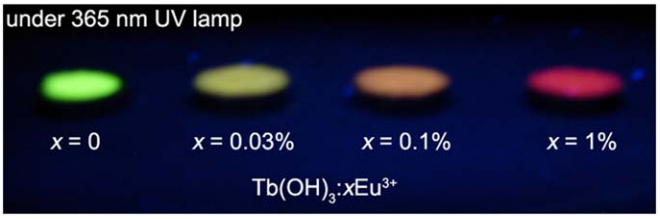

Fig. 7. Luminescent photographs for the $Tb(OH)_3$:xEu^{3+} samples (x=0–1 mol%). Here, a 365 nm ultraviolet lamp was used as an excitation source, and the samples were put onto filter paper in a dark room.

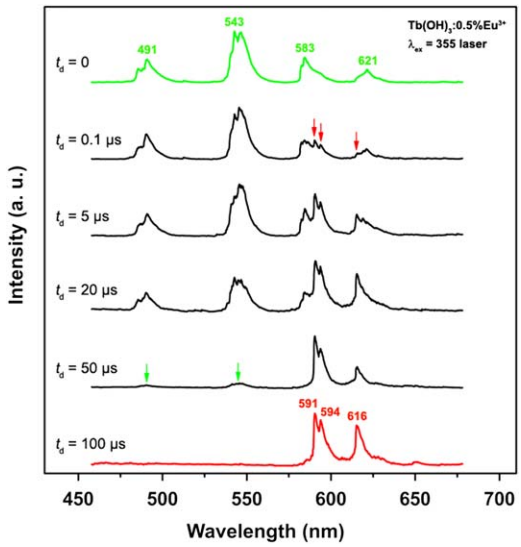

Fig. 8. Time-resolved PL emission spectra of the $Tb(OH)_3$:0.5 mol%Eu^{3+} sample (λ_{ex}=355 nm laser).

tion, which can be seen clearly from the photographs of the $Tb(OH)_3$:xEu^{3+} samples presented in Fig. 7 (where a 365 nm UV lamp was used as an excitation source and the samples were put onto filter paper in a dark room).

To study the energy transfer process from Tb^{3+} to Eu^{3+} in $Tb(OH)_3$:Eu^{3+} in more detail, time-resolved emission spectra of $Tb(OH)_3$:0.5 mol% Eu^{3+} were measured by excitation into the Tb^{3+} band with a 355 nm laser. The emission spectra collected at different delay times (t_d) are shown in Fig. 8. When t_d=0 μs, only the characteristic emission of Tb^{3+} is observed; no Eu^{3+} emission is present because the excitation energy of Tb^{3+} has not been transferred to Eu^{3+} at this time. When t_d=0.1 μs, the emission of Tb^{3+} starts to decrease accompanied by the presence of Eu^{3+} emissions (red arrows in Fig. 8) due to the energy transfer from Tb^{3+}. The emission of Tb^{3+} decreases gradually with further increase of the delay time (green arrows in Fig. 8), whereas that of Eu^{3+} begins to increase due to transfer of more excitation energy from Tb^{3+} to Eu^{3+}. When t_d=100 μs, the emission of Tb^{3+} disappears, and the emission spectrum contains exclusively that of Eu^{3+}. When $t_d > 100$ μs, the Eu^{3+} emission also begins to decay gradually and disappears finally due to the depopulation of the excited states (Figures are not shown due to the limited space). Actually, we cannot conclude whether the energy transfer from Tb^{3+} to Eu^{3+} is of radiative type or nonradiative type just from the time-resolved emission spectra shown in Fig. 8. In general, radiative energy transfer only occurs in some crystals and the energy transfer among rare earth ions is of nonradiative type, that is, the resonant energy transfer occurs via the electric dipole–dipole or electric dipole–quadrupole interactions [3,7]. The same

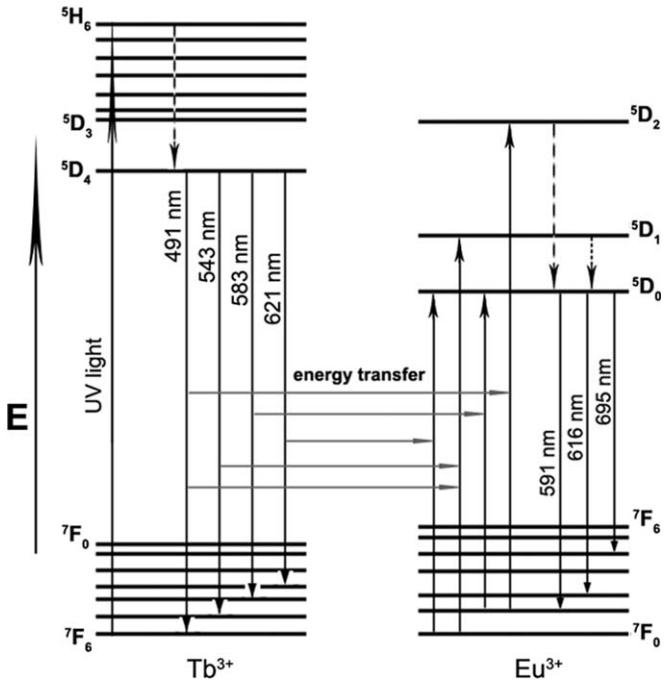

Fig. 9. Scheme of energy transfer from Tb^{3+} to Eu^{3+}. The up solid arrows represent photoexcitation, the down solid arrows mean emission, and the down dash arrows denote multiphonon relaxation.

situation (nonradiative energy transfer) also holds for the energy transfer from Tb^{3+} to Eu^{3+} in our present work, which was well demonstrated in other hosts in previous reports [9–14,41,42].

A summary of the emission and energy transfer process of Tb^{3+} and Eu^{3+} in $Tb(OH)_3$:Eu^{3+} is shown schematically in Fig. 9 [9–14,41,42]. First, electrons on Tb^{3+} ions are excited from the ground state ($^7F_6$) to the higher excited states ($^5H_6$, $^5D_3$, $^5D_4$…) by UV light. Subsequently, these electrons relax to the lowest excited state $^5D_4$ through multiphonon relaxation then either return to the ground states to produce the Tb^{3+} emissions ($^5D_4 \rightarrow {}^7F_{6,\,5,\,4,\,3}$), or transfer their excitation energy from $^5D_4$ (Tb^{3+}) level to the higher excited energy levels of Eu^{3+} ($4f^6$) through cross relaxation, which relax to the $^5D_0$ (Eu^{3+}) level, where the red emission ($^5D_0 \rightarrow {}^7F_{1,\,2,\,4}$) takes place. Because the $^5D_4 \rightarrow {}^7F_{6,\,5,\,4,\,3}$ emission of Tb^{3+} is effectively overlapped with the $^7F_{0,\,1} \rightarrow {}^5D_{0,\,1,\,2}$ absorption of Eu^{3+}, the energy transfer from Tb^{3+} to Eu^{3+} is very efficient in general [7]. Moreover, the hexagonal crystal structure of $Tb(OH)_3$ also favors the energy transfer from Tb^{3+} to Eu^{3+} [14,41,42].

According to the model we proposed above, if Tb^{3+} ion was excited from $^7F_6 \rightarrow {}^5D_4$, there should be energy transfer from the excited $^5D_4$ level of Tb^{3+} to the $^5D_{0,\,1,\,2}$ level of Eu^{3+} in $Tb(OH)_3$:Eu^{3+} sample. Upon excitation into the $^7F_6 \rightarrow {}^5D_4$ transition of Tb^{3+} at 490 nm, the emission spectra of $Tb(OH)_3$:0.5%Eu^{3+}, $Tb(OH)_3$, and $Eu(OH)_3$ are presented in Fig. 10 for comparison. The emission spectrum of the $Tb(OH)_3$:0.5%Eu^{3+} sample obtained by excitation with 490 nm ($^7F_6 \rightarrow {}^5D_4$ of Tb^{3+}) has principally the same feature as that of monitoring at 382 nm (Fig. 6), and no emission is observed for pure $Eu(OH)_3$. This further demonstrates that Tb^{3+} ion may act as a good energy donor, from which energy can be transferred to an acceptor Eu^{3+}.

4. Conclusions

In summary, we have demonstrated that a simple, mild and catalyst-/template-free hydrothermal method for synthesis of $Tb_{(1-x)}(OH)_3$:xEu^{3+} nanorods directly without reductive ambi-

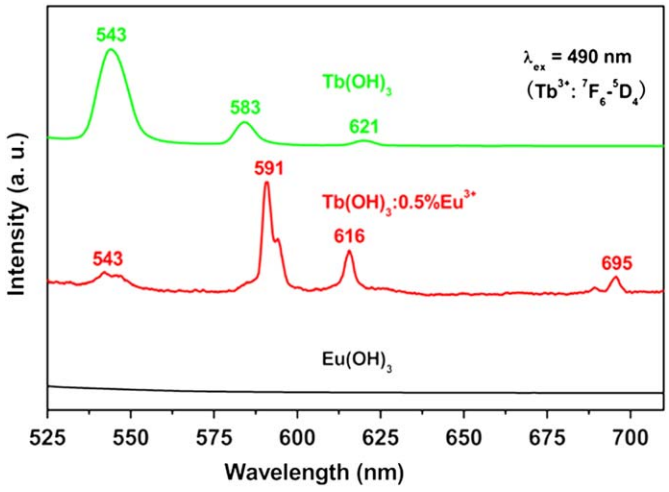

Fig. 10. Emission spectra of the $Tb(OH)_3$:0.5 mol%Eu^{3+}, $Tb(OH)_3$, and $Eu(OH)_3$ samples upon excitation into the $^7F_6 \rightarrow {}^5D_4$ transition of Tb^{3+} at 490 nm, respectively.

ence for protection. The formation mechanisms for the $Tb(OH)_3$:Eu^{3+} 1D structure have been proposed on an anisotropic growth nature resulting from the hexagonal crystal structure of lanthanide hydroxides. An efficient energy transfer can occur from Tb^{3+} to Eu^{3+} in $Tb(OH)_3$ host for the first time, which is ascribed to the energy overlap between Tb^{3+} and Eu^{3+} (Tb^{3+}: $^5D_4 \rightarrow {}^7F_{6,\ 5,\ 4,\ 3} \langle = \rangle$ Eu^{3+}: $^7F_{0,\ 1} \rightarrow {}^5D_{0,\ 1,\ 2} + \Delta E$) and hexagonal crystal structure of $Tb(OH)_3$ host. By controlling the doping concentration of Eu^{3+} (x=0–3 mol%), the luminescent colors could be modified from green, yellow, orange, to red easily because of different composition of emissions of Tb^{3+} and Eu^{3+} resulted from different energy efficiency at different doping concentration of Eu^{3+}. The study opens a novel pathway for tuning the luminescence properties by energy transfer.

Acknowledgments

This project is financially supported by National Basic Research Program of China (2007CB935502, 2010CB327704), the National Natural Science Foundation of China (NSFC 50702057, 50872131, 00610227), the Doctoral Foundation of Southwest University (SWU109013), and the Basic Research Foundation of Southwest University (XDJK2009C008).

References

[1] M. Yu, J. Lin, J. Fu, H.J. Zhang, J. Mater. Chem. 13 (2003) 1413.
[2] J.A. Capobianco, F. Vetrone, J.C. Boyer, A. Speghini, M. Bettinelli, Opt. Mater. 19 (2002) 259.
[3] B.G. Lasse, B.C. Grabmaier, Luminescent Materials, Springer-Verlag, Berlin, Heideberg, 1994.
[4] C. Feldmann, T. Jüstel, C.R. Ronda, P.J. Schmidt, Adv. Funct. Mater. 13 (2003) 511.
[5] R.C. Evans, L.D. Carlos, P. Rocha, J. Douglas, J. Mater. Chem. 18 (2008) 1100.
[6] [a] W.J. Yang, T.M. Chen, Appl. Phys. Lett. 88 (2006) 101903;
[b] T. Hayakawa, A. Hiramitsu, M. Nogami, Appl. Phys. Lett. 82 (2003) 2975.
[7] E. Nakazawa, S. Shionoya, J. Chem. Phys. 47 (1976) 3211.
[8] L.P. Johnson, J.E. Geusic, L.C. Van Uitert, Appl. Phys. Lett. 8 (1966) 200.
[9] W.W. Holloway, M. Kestigian, R. Newman, Phys. Rev. Lett. 11 (1963) 458.
[10] W. Chen, R. Sammynaiken, Y. Huang, J. Appl. Phys. 88 (2000) 1424.
[11] T. Kim Anh, T. Ngoc, P. Thu Nga, V.T. Bitch, P. Long, W. Strek, J. Lumin. 39 (1988) 215.
[12] A. Moadhen, H. Elhouichet, B. Canut, C.S. Sandu, M. Oueslati, J.A. Roger, Mater. Sci. Eng. B 105 (2003) 157.
[13] Z.J. Hang, H.H. Chen, X.X. Yang, J.T. Zhao, Mater. Sci. Eng. B 145 (2007) 34.
[14] W.H. Di, X.J. Wang, P.F. Zhu, B.J. Chen, J. Solid State Chem. 180 (2007) 467.
[15] J. Yang, C.M. Zhang, C.X. Li, Y.N. Yu, J. Lin, Inorg. Chem. 47 (2008) 7262.
[16] Y.N. Xia, P.D. Yang, Y.G. Sun, Y.Y. Wu, B. Mayers, B. Gates, Y.D. Yin, F. Kim, H.Q. Yan, Adv. Mater. 15 (2003) 353.
[17] X. Wang, Y.D. Li, Angew. Chem. Int. Ed. 41 (2002) 4790.
[18] A. Ghezelbash, M.B. Sigman Jr., B.A. Korgel, Nano Lett. 4 (2004) 537.
[19] Y.D. Li, X.F. Duan, Y.T. Qian, L. Yang, M.R. Ji, C.W. Li, J. Am. Chem. Soc. 119 (1997) 7869.
[20] Q. Peng, Y.J. Dong, Z.X. Deng, Y.D. Li, Inorg. Chem. 41 (2002) 5249.
[21] X.F. Duan, C.M. Lieber, Adv. Mater. 12 (2000) 298.
[22] B. Gates, Y.D. Yin, Y.N. Xia, J. Am. Chem. Soc. 122 (2000) 12582.
[23] M.H. Huang, S. Mao, H. Feick, H.Q. Yan, Y.Y. Wu, H. Kind, E. Weber, R. Russo, P.D. Yang, Science 292 (2001) 1897.
[24] [a] T. Kasuga, M. Hiramatsu, A. Hoson, T. Sekino, K. Niihara, Adv. Mater. 11 (1999) 1307;
[b] X. Wang, Y.D. Li, J. Am. Chem. Soc. 124 (2002) 2880.
[25] Z.W. Pan, Z.R. Dai, Z.L. Wang, Science 291 (2001) 1947.
[26] J. Yang, C.X. Li, Z.Y. Cheng, X.M. Zhang, Z.W. Quan, C.M. Zhang, J. Lin, J. Phys. Chem. C 111 (2007) 18148.
[27] A.W. Xu, Y.P. Fang, L.P. You, H.Q. Liu, J. Am. Chem. Soc. 125 (2003) 1494.
[28] X. Wang, Y.D. Li, Chem. Eur. J. 9 (2003) 5627.
[29] J.C. Wang, Q. Liu, Q.F. Liu, J. Mater. Chem. 15 (2005) 4141.
[30] J. Zhang, Z.G. Liu, J. Lin, J. Fang, Cryst. Growth Des. 5 (2005) 1527.
[31] Q. Tang, Z.P. Liu, S. Li, S.Y. Zhang, X.M. Liu, Y.T. Qian, J. Cryst. Growth 259 (2003) 208.
[32] Y.P. Fang, A.W. Xu, L.P. You, R.Q. Song, J.C. Yu, H.X. Zhang, Q. Li, H.Q. Liu, Adv. Funct. Mater. 13 (2003) 955.
[33] F. Tao, Z.J. Wang, L.Z. Yao, W.L. Cai, X.G. Li, Nanotechnology 17 (2006) 1079.
[34] Q. Tang, J.M. Shen, W.J. Zhou, W. Zhang, W.C. Yu, Y.T. Qian, J. Mater. Chem. 13 (2003) 3103.
[35] J. Yang, C.X. Li, X.M. Zhang, Z.W. Quan, C.M. Zhang, H.Y. Li, J. Lin, Chem. Eur. J. 14 (2008) 4336.
[36] J. Yang, C.M. Zhang, L.L. Wang, Z.Y. Hou, S.S. Huang, H.Z. Lian, J. Lin, J. Solid State Chem. 181 (2008) 2672.
[37] G. Wang, Z.D. Wang, Y.X. Zhang, G.T. Fei, L.D. Zhang, Nanotechnology 15 (2004) 1307.
[38] X. Wang, Y.D. Li, Inorg. Chem. 45 (2006) 7522.
[39] G. Du, G.V. Tendeloo, Nanotechnology 16 (2005) 595.
[40] K.S. Thomas, S. Singh, G.H. Dieke, J. Chem. Phys. 38 (1963) 2180.
[41] T. Kim Anh, W. Strek, J. Lumin. 42 (1988) 205.
[42] G. Schierning, M. Batentschuk, A. Osvet, A. Winnacker, Radiat. Meas. 38 (2004) 529.
[43] M. Yu, J. Lin, J. Fu, Y.C. Han, Chem. Phys. Lett. 371 (2003) 178.
[44] K. Riwotzki, H. Meyssamy, A. Kornowski, M. Haase, J. Phys. Chem. B 104 (2000) 2824.